Chemistry–A European Journal
Research Article
doi.org/10.1002/chem.202203667
Chemistry Europe
European Chemical Societies Publishing
www.chemeurj.org

Ability of Azathiacyclen Ligands To Stop Cu(Aβ)-Induced Production of Reactive Oxygen Species: [3N1S] Is the Right Donor Set

Kyangwi P. Malikidogo[+],[a, d] Marielle Drommi[+],[a] Elena Atrián-Blasco,[a, e] Jan Hormann,[b] Nora Kulak,[b, c] Charlène Esmieu,*[a] and Christelle Hureau*[a]

Abstract: Alzheimer's disease (AD) is an incurable neurodegenerative disease that leads to the progressive and irreversible loss of mental functions. The amyloid beta (Aβ) peptide involved in the disease is responsible for the production of damaging reactive oxygen species (ROS) when bound to Cu ions. A therapeutic approach that consists of removing Cu ions from Aβ to alter this deleterious interaction is currently being developed. In this context, we report the ability of five different 12-membered thiaazacyclen ligands to capture Cu from Aβ and to redox silence it. We propose that the presence of a sole sulfur atom in the ligand increases the rate of Cu capture and removal from Aβ, while the kinetic aspect of the chelation was an issue encountered with the 4N parent ligand. The best ligand for removing Cu from Aβ and inhibiting the associated ROS production is the 1-thia-4,7,10-triazacyclododecane [3N1S]. Indeed the replacement of more N by S atoms makes the corresponding Cu complexes easier to reduce and thus able to produce ROS on their own. In addition, the ligand with three sulfur atoms has a weaker affinity for Cu^{II} than Aβ, and is thus unable to remove Cu from CuAβ.

Introduction

Alzheimer's disease (AD) is the most widespread neurodegenerative disease.[1] AD is undoubtedly a multifactorial disease, but displays well-defined pathological markers as the Tau tangles or the amyloid plaques. These plaques are made of the amyloid beta peptides (Aβ) that aggregate according to a process named as the amyloid cascade.[2] This process spans from the secretion of Aβ from the amyloid precursor protein (APP) to its oligomerisation, fibrillation and the final plaques formation.[3,4] It is commonly admitted that Aβ is mainly composed of 40/42 amino acid residues. The first 16 residues encompass metal ions binding sites.[5,6] In line with this ability, it has been reported that the plaques are enriched in metal ions, Zn, Fe and Cu bound to Aβ.[7–12] More than only modifying the metal-free aggregation of Aβ, Cu bound to Aβ is associated to the catalytic production of reactive oxygen species (ROS), implicated in the overall oxidative stress observed in AD brain.[5,13]

Years of investigations have led to the determination of the Cu coordination sites within the peptide, but the elucidation of the ROS production mechanism is still in progress. Within the peptide, Cu^{II} is coordinated by the N-terminal amine, the adjacent carbonyl group from the peptide backbone, and two imidazole rings from the His residues in a square-planar geometry with an apparent affinity constant of 10^9–10^{10} M^{-1} at pH 7.4.[14–16] ROS are believed to be produced by an "in between state" (IBS) that the peptide can adopt when bound to Cu.[17,18] In this particular geometry Cu is able to redox cycle very fast in the presence of a reductant (e.g., ascorbate) and O_2, leading to the incomplete reduction of O_2 and the formation of ROS.[18]

In order to disrupt the deleterious coordination interaction between Cu ions and Aβ peptide, chemists have developed Cu ligands able to remove Cu from Aβ and redox silence it.[19–21] Among the family of molecules studied in this context, azamacrocyclic ligands hold an important place, including the

[a] Dr. K. P. Malikidogo,[+] M. Drommi,[+] Dr. E. Atrián-Blasco, Dr. C. Esmieu, Dr. C. Hureau
LCC-CNRS, Université de Toulouse, CNRS
31400 Toulouse (France)
E-mail: christelle.hureau@lcc-toulouse.fr
charlene.esmieu@lcc-toulouse.fr
Homepage: https://hureaulab.wixsite.com/equipeflcc/christelle-hureau-1
https://hureaulab.wixsite.com/equipeflcc/charl%C3%A8ne-esmieu

[b] Dr. J. Hormann, Prof. Dr. N. Kulak
Institut für Chemie und Biochemie, Freie Universität Berlin
Fabeckstr. 34/36, 14195 Berlin (Germany)

[c] Prof. Dr. N. Kulak
Institut für Chemie
Otto-von-Guericke-Universität Magdeburg
Universitätsplatz 2, 39106 Magdeburg (Germany)

[d] Dr. K. P. Malikidogo[+]
Université Grenoble Alpes
DCM (UMR 5250) - CNRS and CEA, IRIG, LCBM (UMR 5249)
Grenoble (France)

[e] Dr. E. Atrián-Blasco
Instituto de Nanociencia y Materiales de Aragón (INMA)
CSIC-Universidad de Zaragoza
Zaragoza 50009 (Spain)

[+] These authors contributed equally to this work.

Supporting information for this article is available on the WWW under https://doi.org/10.1002/chem.202203667

Part of a Special Collection for the 8th EuChemS Chemistry Congress 2022 consisting of contributions from selected speakers and conveners. To view the complete collection, visit 8th EuChemS Chemistry Congress.

simplest cyclen (1,4,7,10-tetraazacyclododecane, [12]aneN4) and cyclam (1,4,8,11-tetraazacyclotetradecane, [14]aneN4) ligands.[19] The use of cyclen and cyclam ligands was a relevant choice in AD context due to i) their ability to remove Cu from CuAβ,[22] and ii) to form kinetically inert complexes in biologically relevant media,[22] iii) their water solubility and iv) their high tunability (binding atoms, pendant arms…). These properties have been clearly established through their wide use in pharmaceutical chemistry, as therapeutic agents and/or for diagnostic imaging.[23]

More precisely, in an AD context, cyclen,[24] cyclam[25] and their mono or bis N-functionalized derivatives (*N*-(2-(pyridin-2-yl)ethyl)acetamide[26] or methylpicolinate[22]) have been used for their high ability to form Cu^{II} complexes with good thermodynamic stability and kinetic inertness. They have been used as modulators of the metal-induced $A\beta_{40}$ aggregation; in particular, they seem able, at super-stoichiometry, to inhibit $CuA\beta_{40}$ aggregation, disassemble $CuA\beta_{40}$ aggregates and restore its metal free random coil conformation.[24–26] Moreover, it has been recently shown, that the conjugation of cyclen to silica nanoparticles as delivery carriers was a successful strategy to improve the blood brain barrier penetration for such hydrophilic small molecules. Additionally, it has been demonstrated that the silica-cyclen conjugates and their Zn^{II} or Cu^{II} complexes were nontoxic towards the cells.[24]

An effect against the CuAβ-induced ROS formation is also reported for those ligands.[22,24] In a previous study, the removal of Cu^{II} from CuAβ by cyclen has been investigated and has shown that the efficiency in Cu^{II} removal was impeded by kinetic issues.[22] Cyclen was unable to stop the ROS production when added to a mixture of CuAβ, O_2 and ascorbate under ROS producing conditions, that is, after the production of ROS was started. The reduction of $Cu^{II}A\beta$ was faster than the Cu^{II} removal by the cyclen thus allowing the production of ROS. The addition of methylpicolinate pendant arms on the azamacrocycle accelerates the Cu^{II} capture from Aβ and makes the ligand efficient against ROS production in contrast to the parent cyclen. We established here a new strategy to overcome the ligand kinetic efficiency that aims at targeting the reduced state of Cu. Indeed, Cu^{I} needs to be removed from Aβ as soon as the reduced $Cu^{I}A\beta$ complex is generated in order to avoid its quick and harmful reaction with O_2, and thus ligands able to withdraw Cu^{I} from Aβ are also highly appropriate. Following the HSAB theory, the addition of S donor atoms into the azamacrocycle ligands appeared as a valuable choice in this strategy and should help to increase the affinity of the macrocyclic ligands for the Cu^{I}. To efficiently avoid the ROS production, the generated Cu^{I}-azamacrocyclic complexes will need either to be air stable or to be oxidized to form a corresponding Cu^{II} complex resistant to ascorbate reduction.

However, as a side effect, the addition of S donor atoms into the macrocycle will decrease the reduction potential of the Cu^{II} complexes generated.[27–29] The parent Cu^{II} cyclen complexes are resistant to the reduction by biologically relevant reductant as ascorbate[22] but adding S donor atoms into the coordination sphere will make the Cu^{II} complexes easier to reduce[27–29] and the complexes themselves unable to inhibit the redox cycling of Cu in the presence of O_2 and ascorbate. Hence, a fine tuning needs to be found between the Cu^{I} affinity constant and the redox potential of the Cu-complexes; while increasing the number of sulfur atoms should help the Cu^{I} removal, the $Cu^{II/I}$ redox potential needs to be controlled in order to inhibit the ROS production. These two aspects will be illustrated in this article.

In this report, the effect of the one by one replacement of nitrogen atoms by sulfur atoms in the cyclen framework, against CuAβ-induced ROS production was investigated and compared to the parent cyclen [12]ane, 4N (**L1**). Four thiaazacyclen ligands (Figure 1) were evaluated, including the *cis* and *trans* 2N2S species in order to find the most efficient set of donor atoms in preventing CuAβ-induced ROS production. **L1**: cyclen, 4N; **L2**: 1-thia-4,7,10-triazacyclododecane or 3N1S; **L3**: 1,7-dithia-4,10-diazacyclododecane or NSNS; **L4**: 1,4-dithia-7,10-diazacyclododecane or 2N2S; **L5**: 1,4,7-trithia-10-azacyclododecane or 1N3S. For solubility reasons, the 1,4,7,10-tetrathiaazacyclododecane 4S, was excluded from the study.

For all the five ligands, the Cu^{I} and Cu^{II} complexes were synthetized in situ and characterized by UV-vis, EPR and X-ray absorption near-edge structure (XANES) spectroscopies and electrochemistry. The effect of the substitution of N by S atoms on the different spectroscopic and electrochemical parameters was evaluated. The ability of the different ligands to remove Cu from the $CuA\beta_{16}$ complex was monitored by UV-vis and EPR for Cu^{II} and XANES for Cu^{I}. Then, the effect of **L1**-**5** on the $CuA\beta_{16}$-induced ROS production was evaluated in test tubes. We show that **L5** is able to target and stabilize Cu^{I} but the formed complex Cu^{I}**L5** is not air stable and form Cu^{II}**L5** that can be further reduced by ascorbate. Hence, Cu**L5** produces ROS. The results obtained also show that the addition of a sole S atom into the cyclen framework (**L2**) makes possible the Cu removal from $A\beta_{16}$ and its redox silencing in contrast to the parent cyclen.

Figure 1. Schematic representation of the different **L*i*** ligands studied.

Results and Discussion

Characterization of the CuLi complexes

UV-vis

The UV-vis spectra of the five complexes obtained upon Cu^{II} binding of **L1**-**5** at pH 7.4 are depicted in Figure 2A and parameters are reported in Table 1. At this pH, the titration of Cu^{II} to any **L*i*** ligand shows the formation of 1:1 complex (Figure S1 in the Supporting Information). All the ligands display a transition band in the d–d region characteristic of the formation of Cu^{II} complexes. A bathochromic shift is observed going from the 4N to the 1N3S ligand (Figures 2A and S2). The presence of sulfur atoms decreases the energy of the d-d transition in line with a better electron-donating characteristic of sulfur versus nitrogen atoms. As well, the molar extinction coefficient (ε) of the band increases as a function of the number of sulfur atoms (Figures 2A and S2), except for the NSNS (**L3**) ligand. This variation could arise from a difference in the geometry of this complex (see below). An intense band is observed in the 300–400 nm region for the S-containing complexes which is assigned to a S→Cu^{II} charge transfer transition (LMCT) as previously reported (Figure 2A),[30–32] while the band of Cu^{II}**L1** at 271 nm is assigned to a N→Cu^{II} charge transfer transition (LMCT).[31,32]

EPR

EPR spectra of each Cu^{II} complex formed in situ at pH 7.4 are depicted in Figures 2B and S4 (as a function of pH) and EPR parameters (*g* values and hyperfine couplings, A) are given in Table 1. Two sets of different EPR parameters are clearly observable for Cu^{II}**L3** (Cu^{II}NSNS). This feature is indicative of the presence of two different complexes in the frozen sample. One of the species (named Cu^{II}**L3**^{a}) shares almost the same EPR parameters than the one recorded for Cu^{II}**L4**. The other species is named Cu^{II}**L3**^{b}. The EPR parameters have been directly measured on the spectra from the position of the second and third hyperfine lines, which are clearly defined due to the use of isotopically pure ^{65}Cu source. The $g_{\|}$ value corresponds to the

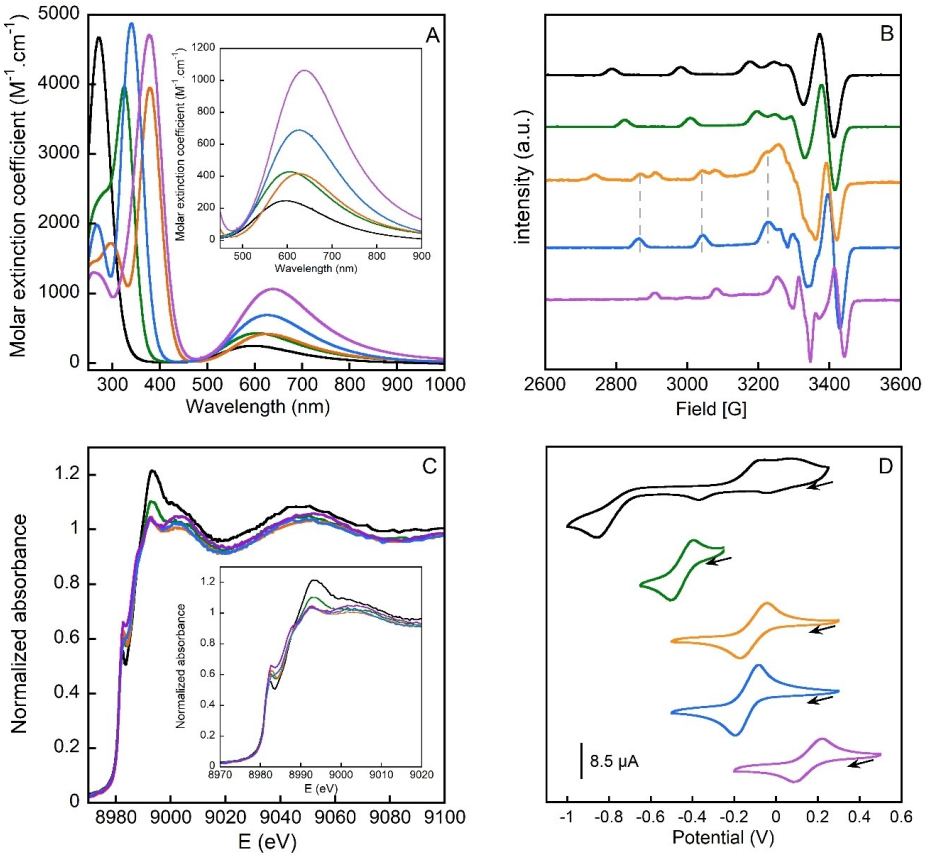

Figure 2. Characterization of the Cu^{II}**L*i*** complexes, Cu^{II}**L1** (black), Cu^{II}**L2** (green), Cu^{II}**L3** (orange), Cu^{II}**L4** (blue) and Cu^{II}**L5** (violet). A) UV-vis spectra (molar extinction coefficient vs. wavelength), the inset shows an enlargement of the d–d transition region; [**L*i***] = 290 µM, [Cu^{II}] = 240 µM, [HEPES] = 100 mM, pH 7.4, *T* = 25 °C. B) X-band EPR spectra, vertical dotted gray lines indicate that a species found in the Cu^{II}**L3** mixture has the same coordination sphere as in Cu^{II}**L4**; [**L*i***] = 600 µM, [$^{65}Cu^{II}$] = 500 µM, [HEPES] = 100 mM, pH 7.4, 10% of glycerol as cryoprotectant, 120 K. C) Normalized Cu^{I} XANES spectra; [**L*i***] = 1 mM, [Cu] = 0.9 mM, [HEPES] = 50 mM, pH 7.4. Copper was reduced with dithionite at 10 mM, and the solution was kept under argon; glycerol (10% *v*/*v*) was used as a cryoprotectant, *T* = 20 K. D) Cyclic voltammograms, arrows indicate the starting point (the open circuit potential) [**L*i***] = 600 µM, [Cu^{II}] = 500 µM, [HEPES] = 100 mM, pH 7.4, scan rate 100 mV s^{-1} at room temperature, the reference electrode is SCE (+0.242 mV *vs.* NHE).

Table 1. Redox potentials, UV-vis and EPR parameters determined for Cu^{II}**L*i*** complexes.

Ligand	$E_{1/2}$ vs. NHE [V]	UV-Vis LMCT λ_{max} [nm]	ε [M^{-1} cm^{-1}]	d-d λ_{max} [nm]	ε [M^{-1} cm^{-1}]	EPR[a] $g_{\parallel}$ $g_{\perp}$; $g_{\parallel}$	$A_{\parallel}$ [10^4 cm^{-1}] $A_{\perp}$;$A_{\parallel}$ [10^4 cm^{-1}]
L1		271	4700	590	247	2.20	200
						2.046;2.197	*17;199*
L2	−0.21	325	4000	605	430	2.18	191
						2.044;2.180	*14;190*
						2.16	182 (a)
						2.039;2.160	*14;175*
L3	0.14	379	4000	625	420	2.27	180 (b)
						2.049;2.258	*14;177*
L4	0.11	341	5000	627	690	2.16	181
						2.039;2.160	*14;182*
L5	0.40	378	4700	637	1100	2.13	172
						2.039;2.135	*14;174*

[a] EPR have been measured from ^{65}Cu^{II}; (a) and (b) relate to the two species found in the sample. Data from simulations are given in italics.

half-sum of magnetic field of these two lines and the $A_{\parallel}$ to the field difference between them. In addition, the EPR signatures of the six complexes were fitted (Figure S5) to release the $g_{\parallel}$ and $g_{\perp}$, as well as the corresponding hyperfine values (parameters are collected in Table 1, in italics). It is worth noting that the measurement of these parameters from the position of the second and third hyperfine lines that allows minimization of the second-order effects give very similar data to the simulation. Typical axial spectra ($g_{\parallel} > g_{\perp}$) are observed for all the compounds. Based on the values determined using simulation, the g_{iso} parameter was calculated and plotted as function of the ligand binding site (Figure S3A, Table 1). It mirrors the level of covalence in the Cu^{II} complexes,[33] with higher g_{iso} corresponding to weaker covalence. As previously documented and expected, the addition of sulfur atoms in the coordination sphere of Cu^{II} causes a decrease in both parameters due to the greater electron-donating properties of sulfur atoms than nitrogen atoms.[34] In addition the $A_{\parallel} = f(g_{\parallel})$ values (Figure S3B) follows an linear trend, except for Cu^{II}**L3**^{a} and Cu^{II}**L3**^{b}. The variation in the ($g_{\parallel}$; $A_{\parallel}$) (*x*,*y*) coordinates on that plot is perfectly in line with the replacement of nitrogen by sulfur atoms as described by Peisach and Blumberg.[34] Last the fairly high $A_{\parallel}$ values obtained indicate a square-planar geometry rather than a tetrahedral one. This is in line with the reported crystal structures available for Cu^{II}**L2**.[29,35] Cu^{II}**L3**^{a} has weaker $A_{\parallel}$ values than Cu^{II}**L4** despite having the same first coordination ligands. This indicates that Cu^{II}**L3**^{a} has a stronger tetrahedral distortion than Cu^{II}**L4**.[34,36] Cu^{II}**L3**^{b} has a higher $g_{\parallel}$ value and a smaller $A_{\parallel}$. It has been reported previously that depending on the geometry of the complex, the same set of donor atom could give different $g_{\parallel}$ and $A_{\parallel}$ parameters.[37] Thus, looking at their EPR parameters, Cu^{II}**L3**^{b} could share the same binding site than Cu^{II}**L4** but with a highly strong distortion towards a tetrahedron. Nevertheless, it is more likely that Cu**L3**^{b} has another set of coordinating atoms. To gain insight into the coordination of Cu^{II}**L3**^{b}, EPR spectra were recorded at various pH between 6.4 and 9.1. Increasing the pH is followed by the disappearance of the Cu^{II}**L3**^{a} set of signals (Figure S4). As the formation of Cu^{II}**L3**^{b} is pH-driven, we favor the formation of the Cu^{II}**L3**OH (Cu^{II}**L3**^{b}) complex with a HO^{-} exogenous ligand in the equatorial position concomitantly to the decoordination of an S-atom from the macrocycle ligand in line with Peisach–Blumberg trends,[31,34] rather than the previously described possible change in geometry[37] (Scheme S1). No indication of the existence of these two species can be detected by UV-vis spectroscopy (i.e., only one maximum of absorption, no broadening of the absorption bands). Nevertheless, Cu^{II}**L3** does not follow the trends observed for the other compounds in terms of molar extinction coefficient (Figure S2). This behavior indicates that a rapid exchange exists in solution and that only an average spectrum is observed, which is not the case anymore in the frozen EPR sample in which the different spectra appear resolved. The pH-dependency of the Cu^{II} complexes formed were monitored using EPR (Figure S4) and no modification of the EPR fingerprints was observed in the pH range [5.4; 8.4] for Cu**L*i*** (i = 1, 2, 4) complexes indicating that only one species prevail near neutral pH. For Cu**L5**, at pH above 7.4, new species appear where the $g_{\parallel}$ and $A_{\parallel}$ values indicate a change in the coordination sphere of one or two sulfur atoms by oxygen donor atoms, in line with the likely binding of HO^{-} when increasing the pH and the associated de-coordination of sulfur atoms. In addition, the selectivity of the **L*i*** ligands for Cu^{II} with respect to Zn^{II} and to Fe^{II}, an important parameter to be taken into account has been measured using EPR (Figure S6 for an illustration with **L2**) and is found to be fully appropriate.

XANES

The Cu^{I} coordination by the set of the **L*i*** macrocycles was probed by X-ray near-edge absorption structure (XANES). As expected, the absorption corresponding to the transition from the 1s orbital to the 4p orbitals of the Cu^{I} are observed in the 8980–8985 eV region of the spectrum (Figure 2C). The position and the intensity of the absorption pre-edge peaks is indicative of a three coordinated complexes and the signatures are reminiscent of $[Et_4N]_2[Cu(SC_6H_4\text{-}p\text{-}Cl)_3]$),[38,39] $[(C_6H_5)_4P]Cu(SPh)_3]^{2-}$,[40–42] or Cu(His)$_3$ complexes.[43] Indeed, in trigonal configuration it has been shown that the decrease in intensity corresponds to the splitting of the $4p_{yz}$ orbitals, being higher in energy than the $4p_x$ levels (polarized along the *C*3 axis).[44] Moreover, it has been reported that the

absorption peak is shifted to higher energy (8985 eV) when the Cu^{I} sits in a tetrahedral geometry.[38,44] The shoulder at 8987.5 eV clearly visible for 1N3S could suggest the presence of a tetrahedral coordination as well, reminiscent of $[Cu(C_5H_5NS)_3]_2Cl_2$ complex.[38,45] Twelve-membered ligands are relatively small rings, when incorporating large sulfur atoms it might be too tight to coordinate Cu^{I} with the four heteroatoms of the ring. While the position and intensity of the pre-edge peak don't vary too much depending on **L*i***, the additional features on the higher energy side are affected. The intensity of the high energy features at 8993 eV decreases from 4N to 2N2S. The position and the intensity of the features have been shown by calculations to be dependent on the SCuS angle in three coordinated complexes (120° purely trigonal and 180° T-shape).[38] Similarly to what have been observed for $Cu_2(GSH)_5$ the ratio between the two first absorption peaks of the spectra would suggest a distorted geometry (between T-shape and trigonal). The modification of the spectra with the different ligands would indicate geometry changes due to modification of the donor atoms (N replaced by S) along the series.

Cyclic voltammetry

Cyclic voltammograms of the complexes are shown in Figure 2D, and the redox potential values are given in Table 1. As previously reported Cu**L1** complex exhibits a non-reversible redox process $Cu^{II}\rightleftarrows Cu^{I}$ with a cathodic potential at −0.85 V and an anodic potential at −0.05 V versus SCE. This phenomenon is explained by the release of the Cu^{I} from the ligand as soon as Cu^{II} is reduced.[29,46,47] Conversely, the cyclic voltammograms of Cu**L2**–**L5** show reversible redox processes corresponding to the reduction of Cu^{II} to Cu^{I} and the oxidation of Cu^{I} to Cu^{II} on the reverse scan. The reversibility indicates that the introduction of one sulfur atom is enough to avoid the Cu^{I} release upon the Cu^{II} reduction.[29] The redox potential increases with the number of S atoms inserted into the macrocycle in line with the more donating effect of S atoms compared to N atoms.[27,28]

Again, Cu**L3** exhibits only one redox process; this did not allow the presence of two species (*i.e.*, Cu**L3**^{a} and Cu**L3**^{b}) to be identified, thus indicating the possible existence of a fast equilibrium between Cu**L3**^{a} and Cu**L3**^{b} in solution (faster than the scan rate). Moreover, Cu**L3** and Cu**L4** have almost the same redox potential as previously reported in aqueous[31] and in organic solvent.[48]

Impact of $A\beta_{16}$ on Cu*L*i coordination: determination of the relative affinities

The impact of addition of $A\beta_{16}$ on the Cu^{II} chelation by **L2**-**5** was studied and monitored by UV-vis, EPR and XANES for Cu^{I}. Different behaviors are observed depending on the ligand, which mirror the Cu-relative affinity of $A\beta_{16}$ versus **L2**-**5**. The sixteen first amino-acids of Aβ are implied in Cu coordination, so the C-terminally truncated $A\beta_{16}$ was used in this study, to avoid the complications linked to the aggregation of $A\beta_{40/42}$, which is not considered here.[6] Such peptide ($A\beta_{16}$) is well accepted as a valid model of the full-length peptide with respect to metal ions binding.[49]

The UV-vis spectra of Cu^{II}**L2** (Figure 3A) and Cu^{II}**L4** (Figure S7B) are not modified in the presence of $A\beta_{16}$ pointing out the preservation of Cu^{II}**L2** and Cu^{II}**L4** in solution, linked to a better affinity of **L2** and **L4** for Cu^{II} compared to $A\beta_{16}$. Conversely, a UV-vis spectra modification is observed when $A\beta_{16}$ is added to Cu^{II}**L5** (Figure 3D). The UV-vis characteristic features of Cu^{II}**L5** (absorbance at 378 and 637 nm) disappear almost totally in the presence of $A\beta_{16}$ while keeping a weak absorbance at 625 nm, strongly indicating the disassembly of Cu^{II}**L5** and the formation of $Cu^{II}A\beta_{16}$. $A\beta_{16}$ is thus able to withdraw Cu^{II} from **L5**. **L3** displays an intermediate behavior as $A\beta_{16}$ is able to remove about 50% of Cu^{II} from it (Figure S7A). It has to be noted that the spectra obtained are the same regardless the order of addition of the different chemicals. This direct competition assays are in line with the respective affinity of Cu^{II} for $A\beta_{16}$ on the one hand and **L*i*** on the other (Table S1).

The Cu^{II}-exchange experiments were then monitored by EPR spectroscopy. For **L1**–**L4** (Figure 3B, E and S8), the spectrum obtained in the presence of the three partners resembles neither the $Cu^{II}A\beta_{16}$ spectrum nor the Cu^{II}**L1**–**4** spectra. This result would suggest the formation of a ternary species: $A\beta_{16}$-Cu^{II}**L1**–**4**. For **L1**, **L2** and **L4**, the modification of the signal only appears in the perpendicular region of the spectrum when comparing Cu^{II}**L1**,**2**,**4** spectrum with $A\beta_{16}$-Cu^{II}**L1**,**2**,**4**. Modifications in this area indicate that, first the ligands displace Cu^{II} from $A\beta_{16}$, incorporating the metal ion into the macrocycle ligands, and second, $A\beta_{16}$ would coordinate the Cu^{II} through histidine residues as reported earlier,[50,51] with minimal modification of the equatorial coordination, hence in apical position. In order to verify this hypothesis, imidazole was directly added to the different complexes as a mimic of the histidine residues of $A\beta_{16}$ (Figure S8). The resulting spectra are identical to the ones recorded in the presence of Cu^{II}, **L1**,**2**,**4** and $A\beta_{16}$ indicating that an imidazole group is indeed coordinated to the copper in the presence of $A\beta_{16}$ generating a ternary species, Im-Cu^{II}**L*i*** ($i = 1, 2, 4$). It has to be noted that the ternary species were not seen by UV-vis spectroscopy due to the small spectral modifications induced by the modification on the apical positions. Addition of **L3** to $CuA\beta_{16}$ led to the formation of only one species which is different from $Cu^{II}A\beta_{16}$, Cu^{II}**L3**^{a} and Cu^{II}**L3**^{b}. Nevertheless, the $g_{\parallel}$ values of this new entity is close to the one of Cu^{II}**L3**^{b} which could be compatible with the formation of $A\beta_{16}$-Cu^{II}**L3**^{c} while depopulating the Cu^{II}**L3**^{a} species. Conversely to what has been observed by UV-vis, it seems that **L3** removes entirely Cu^{II} from $A\beta_{16}$ as no $Cu^{II}A\beta_{16}$ signal is seen in EPR. Correlating EPR and UV-vis results might suggest that the presence of Cu^{II}**L3**^{b} allows the formation of one ternary species with $A\beta_{16}$, in line with similar Cu^{II} affinity (Table S1). This new species, $A\beta_{16}$-Cu^{II}**L3**^{c}, would be in equilibrium with Cu^{II}**L3**^{b} and would have too close EPR parameters to be distinguished. The Cu^{II} environment in this ternary species would be N4 with two imidazole rings coming from $A\beta_{16}$ and the two amine groups from **L3** (Scheme S1). This equilibrium would explain why the S→Cu^{II} is seen with a smaller intensity by UV-vis (Figure S7A).

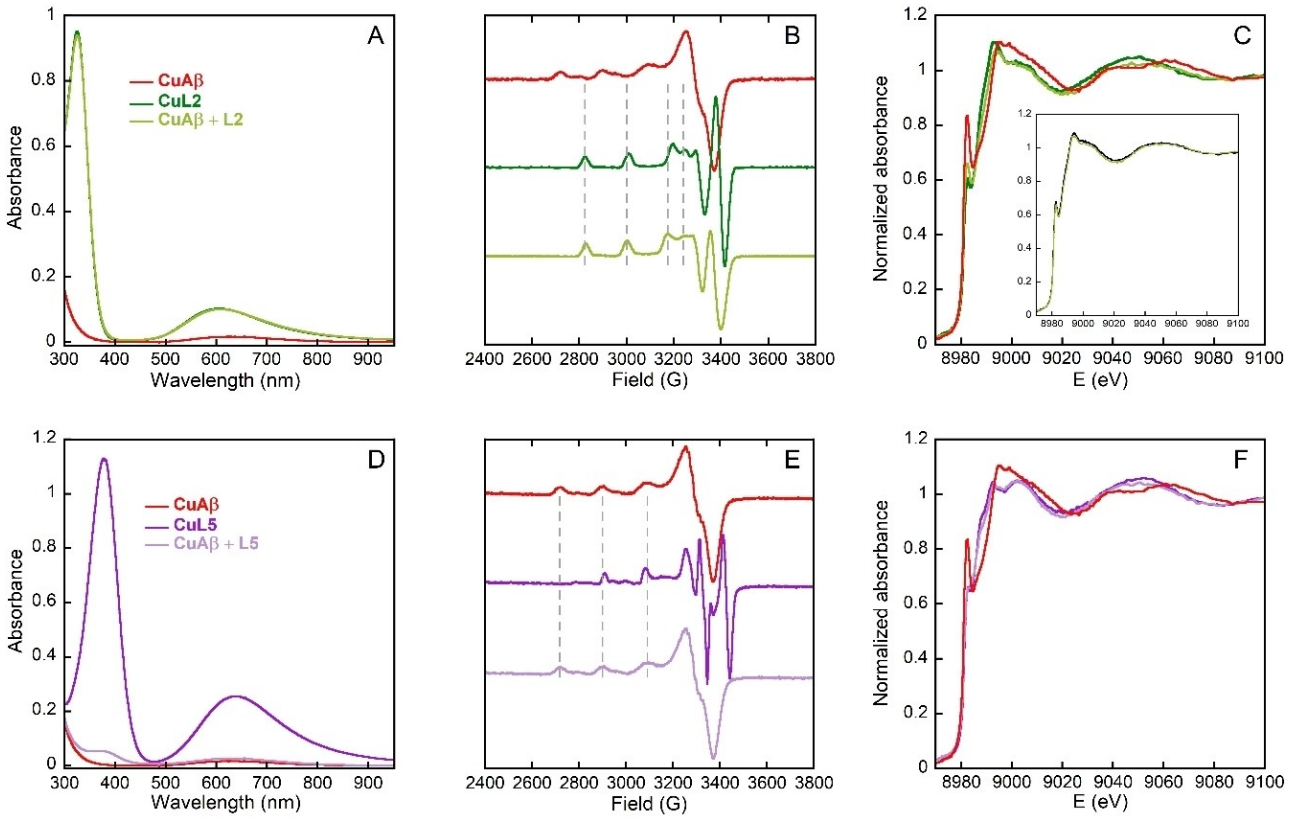

Figure 3. Cu^{II} and Cu^{I} coordination competition between $A\beta_{16}$ and **L2** (top) and between $A\beta_{16}$ and **L5** (bottom) followed by UV-vis (left), X-band EPR (center), and X-ray absorption (right). All the panels contain three curves representing $Cu^{II}A\beta_{16}$ (red), Cu^{II}**L*i*** (green for **L2** and violet for **L5**), $Cu^{II}+A\beta_{16}+$**L*i*** (light green for **L2** and mauve for **L5**). In (C) the inset shows the normalized Cu^{I} XANES spectrum of $Cu^{I}A\beta_{16}+$L2 (light green) and a calculated spectrum (black) with 67% of Cu^{I}**L2** and 33% of $Cu^{I}A\beta_{16}$. Experimental conditions for UV-vis: $[Cu^{II}]=240$ μM, [**L*i***, $A\beta_{16}]=290$ μM, [HEPES] = 100 mM, pH 7.4, $T=25$ °C; for EPR $[^{65}Cu^{II}]=500$ μM, [**L*i***, $A\beta_{16}]=600$ μM, [HEPES] = 100 mM, pH 7.4, 10% of glycerol as cryoprotectant, 120 K; for XANES [**L*i***] = [$A\beta_{16}$] = 1 mM, $[Cu^{II}]=0.9$ mM, [HEPES] = 50 mM, pH 7.4. Copper was reduced with dithionite at 10 mM, and the solution was kept under argon. Glycerol (10% *v*/*v*) was used as a cryoprotectant, $T=20$ K.

This hypothesis is strengthened by the fact that here, the addition of 1 equivalent of imidazole did not allow to reproduce entirely the $A\beta_{16}$-Cu^{II}**L3** signature (Figure S8C), conversely to what has been seen for all the other macrocycles. However adding five equivalents of imidazole leads to virtually the same spectrum as was obtained for $A\beta_{16}$-Cu^{II}**L3**^{c}.

When $A\beta_{16}$ is added to Cu^{II}**L5**, the resulting EPR spectrum resembles the one of $Cu^{II}A\beta_{16}$. $A\beta_{16}$ is thus able to remove Cu^{II} from Cu**L5** which is in total agreement with the results obtained by UV-vis spectroscopy.

XANES was employed to evaluate the Cu^{I} exchange between $A\beta_{16}$ and the ligands. The removal of Cu^{I} from $A\beta_{16}$ by **L1**–**5** was monitored. The fingerprints of Cu^{I}**L3**–**5** are superimposable to the ones obtained for a mixture of $Cu^{I}A\beta_{16}+$**L3**–**5** respectively indicating the complete removal of Cu^{I} by **L3**–**5** (Figures 3F and S9) from $A\beta_{16}$. For **L2** (Figure 3C and S9) the removal of Cu^{I} from $A\beta_{16}$ is not total. It can be calculated from the resulting spectrum that about 67% of the Cu^{I} is linked to the macrocycle ligand and that 33% remains coordinated to $A\beta_{16}$. **L1** which does not have any S atom is not able to remove Cu^{I} from $A\beta_{16}$ (Figure S9). Those results are in line with the HSAB theory, the more sulfur-rich the ligand is, that is, a soft base, the higher affinity it has for Cu^{I} which is a soft acid.

As a brief summary, **L2**–**4** are able to remove Cu^{II} from $A\beta_{16}$ but are probably forming ternary species with the Cu^{II} linked into the macrocycle ligand in equatorial position and by a histidine residue of $A\beta_{16}$ in axial position (at concentration above 200 μM). **L3**–**4** are able to fully remove Cu^{I} from $A\beta_{16}$ while **L2** is only able to remove it partially (67%). Conversely, **L5** is able to remove Cu^{I} but is not able to withdraw Cu^{II} from $A\beta_{16}$.

ROS experiments

The ability of **L2**–**5** to prevent and stop ROS production was investigated in the absence and the presence of $A\beta_{16}$ peptide. Results are presented in Figures 4 and S10–S13. The impact of cyclen (**L1**) on ROS production is also reported as a reference experiment.

Firstly, the ability of the ligands to stop the ROS production by their own was investigated with an ascorbate (Asc) consumption assay followed by UV-vis. This is a commonly used test.[22,52–54] It has been previously shown that the Asc

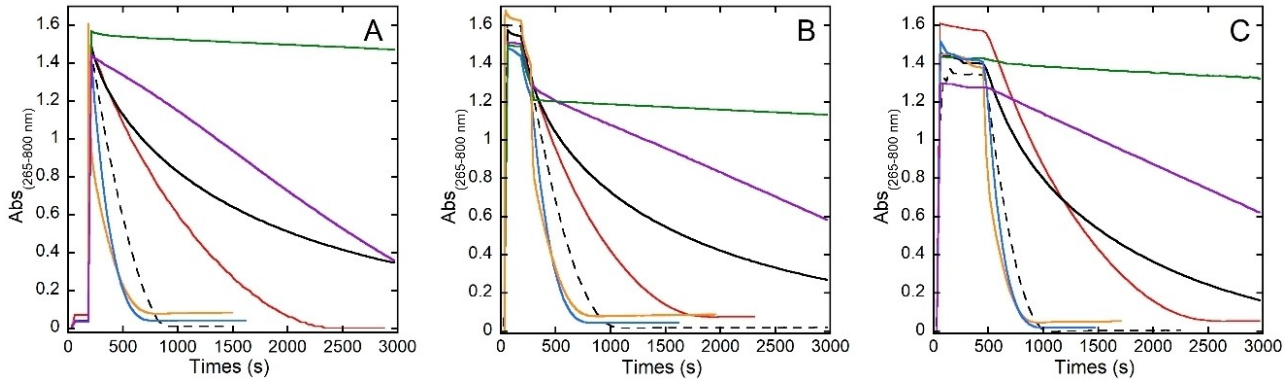

Figure 4. Kinetics of ascorbate consumption in the presence of $A\beta_{16}$ followed by UV-visible spectroscopy at 265 nm starting from A) Cu^{II}, B) $Cu^{II/I}$ and C) Cu^{I}. **L1** (black), **L2** (green), **L3** (orange), **L4** (blue) and **L5** (violet), Cu alone (dashed), $CuA\beta_{16}$ (red). [**Li**, $A\beta_{16}$] = 12 μM, [Cu^{II}] = 10 μM, [Asc] = 100 μM, [HEPES] = 100 mM, pH 7.4, T = 25 °C; for more details see the Supporting Information.

consumption assays perfectly mirrors H_2O_2 formation,[22,52,53,55] $HO^{\bullet}$ release.[19,52,56] The ligands able to avoid the redox cycling of Cu ($Cu^{II}\rightleftarrows Cu^{I}$) and thus preventing the interaction of Cu^{I} with O_2 either by stabilizing the Cu^{II} or the Cu^{I} oxidation states are easily distinguishable by the absence of ascorbate consumption, keeping the absorbance of the ascorbate at 265 nm constant.[22,52,53]

Cu^{II}

In the presence of **L3** and **L4**, ascorbate is quickly consumed (Figure S10). **L3** and **L4**, sharing the particularity that both contain the same set of donor atoms made of two sulfur and two nitrogen atoms, one in the configuration *cis* (2 N2S) and the other one in the configuration *trans* (NSNS), are the less efficient in the series to inhibit the ascorbate consumption. **L3** is even more efficient in catalyzing the production of ROS than Cu alone. As seen in electrochemistry, Cu^{II}**L3** is slightly easier to reduce than Cu^{II}**L4** (0.141 vs. 0.106 V vs. NHE, respectively), and we hypothesize that this explains the differences in ROS production.[57]

L5 slows down the ascorbate consumption (Figure S10); **L5** is better in preventing the ROS production than **L1** (which has been shown to be slow in complexing the Cu^{II}) and both **L3**–**4** with a short incubation time. The Cu^{II}**L5** complex, which is easier to reduce than Cu^{II}**L3**–**4** as seen by electrochemistry, is reduced by ascorbate to the corresponding Cu^{I}**L5** complex. Nevertheless, the ascorbate consumption is slow and might suggest that **L5** is able to stabilize the Cu^{I} redox state and avoid its quick oxidation to Cu^{II}.

L2 shows the best ability to prevent the ROS formation. **L2** is fast in coordinating Cu^{II}, and the resulting Cu^{II}**L2** complex is resistant to ascorbate reduction.

Globally, in the presence of $A\beta_{16}$ the same trends are observed for **L2**–**4** which is in line with their ability to remove Cu^{II} from $A\beta_{16}$ as seen by UV-vis and EPR spectroscopies (Figure 4A). For **L3** two ascorbate rate consumptions are visible and might be related to the time needed to form the $A\beta_{16}$-Cu^{II}**L3**^{b} ternary species (Figures S10–S12). The complex is catalyzing the ROS production very fast at the beginning and a bit slower when the ternary species is formed. A clear decrease in the ability of **L5** to stop the ROS production is observed. Again, this result is totally in line with its lower affinity for Cu^{II} compared to $A\beta_{16}$ as seen by UV-vis and EPR spectroscopy (Figure 3D and E).

Cu^{I} and $Cu^{I/II}$

ROS experiments from Cu^{I} and $Cu^{I}A\beta_{16}$ were carried out as well, and the results are presented in Figures S11 and 4C, respectively. As previously described for Cu^{II}-containing experiments, ascorbate is quickly consumed for **L3**–**4** (Figure 4C) regardless the presence of $A\beta_{16}$ (Figure S11). In the presence of Cu^{I}, no ascorbate was consumed for **L2** (Figure 4C) regardless the presence of $A\beta_{16}$ (Figure S11). This means that **L2** is forming an oxygen stable complex or that the Cu^{I}**L2** complex is quickly oxidized to the ascorbate-reduction stable Cu^{II}**L2**. When the UV-vis cuvette is opened to the air, the d-d transition band of Cu^{II}**L2** forms rapidly and quantitatively (Figure S13), thus indicating that Cu^{I}**L2** does not resist to O_2 oxidation. For **L5** in absence of $A\beta_{16}$, the ascorbate consumption is slowed down (Figure S11) indicating that the Cu^{I}**L5** can slowly cycle between the two Cu redox forms. Nevertheless, conversely to what has been observed for **L2**, the d–d transition band does not grow in the presence of air (Figure S13). This phenomenon might indicate that Cu^{I}**L5** is slowly oxidized to Cu^{II}**L5** in line with the slow ascorbate consumption and that when formed, the Cu^{II}**L5** complex is quickly reduced by ascorbate. This result supports the fact that **L5** is able to stabilize Cu in its reduced form. Again, in the presence of $A\beta_{16}$, the ability of **L5** to remove Cu from $A\beta_{16}$ is impaired, resulting in greater ascorbate consumption. It may be envisaged that the small part of Cu^{I}**L5** which is oxidized to Cu^{II}**L5** would transfer its Cu^{II} to $A\beta_{16}$ and that $Cu^{II}A\beta_{16}$ produces ROS, in line with the relative affinity determined by UV-vis and EPR spectroscopies. However, once generated, the $Cu^{I}A\beta_{16}$ can interchange its metal ions with **L5**. To secure the

results of such Cu^{I} experiment, another set up was also used for **L2** and **L5** (taken as examples), in which instead of opening the UV-vis cuvette to air, we added a dioxygen-saturated solution to the Cu^{I} solution. The data obtained are identical (Figure S14).

The same observations can be made from the experiment starting from a mixture of $Cu^{II/I}$ (Figures 4B and S12).

Note, that to secure the fact that the use of $A\beta_{16}$ instead of the full-length $A\beta_{40}$ doesn't induce artefacts in these ROS experiments, we have reproduced those with **L2** and **L5** in the presence of $A\beta_{40}$. The results are the same as with $A\beta_{16}$ (Figure S15).

Kinetic inertness of the formed Cu^{II}L2

Because **L2** is the most suitable ligand, we also evaluated the rate of Cu^{II} release by Cu^{II}**L2** in competition with human serum albumin (HSA) using EPR (Figure S16) and in competition with the no3pa (tris-picolylamine-1,4,7-triazacyclononane) and **L1** ligands using UV-vis light (Figure S17). The Cu^{II}**L2** complex was mixed with one equivalent of each competitor. The experiments give very interesting results, which are i) HSA is not able to extract Cu from Cu^{II}**L2**, in line with the respective Cu^{II} affinity of HSA and **L2** (Table S1) but forms a ternary species reminiscent to the one obtained with imidazole, Im-Cu^{II}**L2**, ii) both no3pa and **L1** are thermodynamically able to remove Cu^{II} from Cu^{II}**L2** in line with respective affinity (Table S1), iii) no3pa is able to remove Cu^{II} from Cu^{II}**L2** with a $t_{1/2}$ of about 10 h; iv) **L1** extracts Cu^{II} from Cu^{II}**L2** but with a very slow rate (compared to no3pa) and a $t_{1/2} > 10$ days. This indicates that when the reaction goes through an association mechanism (in the case of the no3pa ligand, reminiscent of what was previously observed with picolinato-armed cyclen and cyclam ligands[22]), the rate of extraction is fast (hours' time scale). In contrast, when it proceeds according to a dissociation mechanism (in the case of **L1**) it is much slower (a timescale of days). The latter case mirrors the rate of Cu^{II} release by Cu**L2** that is thus extremely slow.

Proposed mechanisms for L2 and L5

Combining all the results, a mechanism describing **L2** and **L5** actions, which are the best ligands of the series, can be proposed (Figure 5). **L2** is a ligand capable of forming Cu^{II}**L2** which is a ROS dead-end complex as it does not generate ROS by its own in the presence of an excess of ascorbate as reductant and O_2. In the presence of $Cu^{II}A\beta_{16}$, **L2** is able to retrieve Cu^{II} from $A\beta_{16}$ and then inhibit the $CuA\beta_{16}$ toxicity through the formation of Cu^{II}**L2**. Starting from $Cu^{I}A\beta_{16}$ or from $Cu^{II/I}A\beta_{16}$, leads to the rapid formation of Cu^{II}**L2** by O_2 oxidation of Cu^{I}**L2**. **L2** is able to remove both Cu^{I} (67%) and Cu^{II} (quantitatively) from $A\beta_{16}$, so it is difficult to determine if **L2** removes Cu^{I} from $A\beta_{16}$ directly or if $Cu^{I}A\beta_{16}$ is oxidized first and then **L2** removes Cu^{II}. Regardless of the pathway, the Cu^{II}**L2** species is generated quickly enough to stop the ROS production.

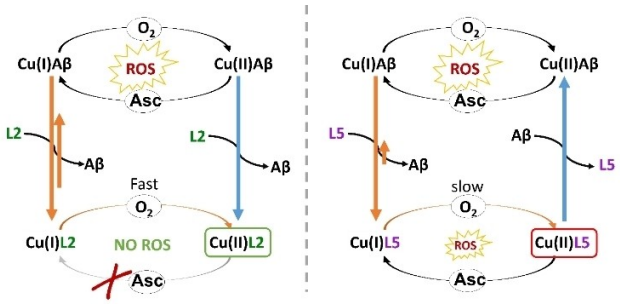

Figure 5. Summary of Cu chelation and ROS production in the presence of $A\beta_{16}$ with **L2** (left) and **L5** (right) illustrating the preferred redox state of Cu for the two ligands.

In the presence of Cu^{II}, **L5** is only able to slow down the ROS production, meaning that ascorbate reduces Cu^{II}**L5**. In the presence of $A\beta_{16}$ the ability of **L5** to slow down the ROS production is almost abolished due to complete formation of the $Cu^{II}A\beta_{16}$ complex over the Cu^{II}**L5** species. Nevertheless, despite the fact that **L5** cannot compete for Cu^{II} in the presence of $A\beta_{16}$ (as shown by EPR) the ascorbate is not consumed as fast as for $Cu^{II}A\beta_{16}$ indicating that an exchange also occurs at the Cu^{I} level.

Conclusions

Chemical properties of the thiaazacyclen ligands in buffered medium at pH 7.4

In this work, we have studied the coordination of Cu^{I} and Cu^{II} to four thiaazacyclen ligands in aqueous medium at pH 7.4. This first step is helpful for studying the complexes further for biological purposes. Although thiaazacyclen macrocycles have been known for decades, their Cu complexes are still poorly studied in buffered aqueous media. During our investigations, it became apparent that deeper physicochemical characterization of the Cu^{I}**L*i*** and Cu^{II}**L*i*** and counterparts with other [N,O,S] sites by EXAFS and multifrequence and pulsed EPR could deserve a full independent benchmark study. The coordination properties of **L2**, **L4** and **L5** follow the expected trend for progressive substitution of N to S atoms into the cyclen scaffold, whereas **L3** shows a peculiar trend. Indeed, for **L3**, two complexes with different parameters are observed by EPR spectroscopy. One set of signals is identical to that of Cu^{II}**L4**, and we thus propose a similar coordination. For the second species, which becomes predominant at higher pH, **L3** probably forms a Cu**L3**OH complex in which the OH replaces one of the macrocycle atoms.

The redox processes of the complexes are reversible with the substitution of the first S atom. The more S atoms are added, the more the $E_{1/2}$ is shifted to higher values from −0.21 to 0.4 V versus NHE for **L1** and **L5** respectively. **L5** is thus able to strongly stabilize Cu^{I}.

Removal of Cu from CuAβ_{16} by the L*i* ligands

Cu chelation competition experiments were conducted followed by spectroscopy with Aβ_{16} and **L*i***. **L1**–**4** are able to remove Cu^{II} totally or partially from Aβ_{16}, whereas **L5** cannot compete with Aβ_{16}. **L3**–**5** are able to remove Cu^{I} totally from Aβ_{16}, whereas **L2** removes it only partially and **L1** cannot. This is fully in line with the HSAB theory.

Effect of Li ligands on CuAβ$_{16}$-induced ROS production

L2 is remarkably efficient in arresting the Cu-induced ROS production regardless the starting Cu redox state. **L2** does not suffer from the slow coordination kinetics encountered with the parent cyclen. The coordination of Cu^{II} is fast, as shown by the ROS experiment starting from Cu^{II}; there is no need for pre-incubation to totally inhibit ROS production. Once Cu^{II}**L2** is formed, it cannot be reduced by ascorbate.

L3 and **L4** are able to remove Cu$^{II/I}$ from Aβ_{16}, but are not able to stop ROS production. Moreover, they favor cycling between Cu^{II} and Cu^{I} compared to free Cu. This phenomenon could be attributed to the redox potential of Cu^{II}**L3** and Cu^{II}**L4** in the appropriate range to be efficiently reduced by ascorbate and oxidized by dioxygen, and by the geometry of the complexes requiring a minimal structural reorganization between the two redox states.

Cu**L5** can produce ROS moderately, as it appears that Cu^{II}**L5** can be reduced by ascorbate and that the Cu^{I}**L5** can be (re)oxidized. Nevertheless, the oxidation by O_2 is slow.

Substitution of N by S atom(s) in the thiaazamacrocycle increases the overall kinetics of Cu capture. At this point it is not possible to conclude by which pathway the Cu^{II} complex is formed after demetallation of CuAβ_{16} species: Cu^{II} is taken out of the Aβ_{16} faster than in absence of S atoms and/or Cu^{I} is taken out of the Aβ_{16} and reoxidized (both rapidly). In the former case, the replacement of a nitrogen by a sulfur atom would have similar kinetic effects as the one previously reported for the addition of picolinato arms to cyclen and/or cyclam ligands,[22] that is to say it allows faster Cu^{II} capture. In the case of the picolinato-armed cyclen or cyclam, this is the duty of this additional moiety. Here in case of sulfur, it might be anticipated that replacement of the nitrogen atoms by the bulkier sulfur induces a less rigid cycle, more prone to distortion to anchor the Cu^{II}.

Changing N for S atoms has two other consequences: i) it significantly changes the redox potential, making some of the Cu**L*i*** complexes able to form ROS on their own and ii) it affects the affinity for both Cu^{I} and Cu^{II}. Hence a good balance should be found between the thermodynamics and kinetics of Cu capture and its redox silencing. In the series studied, **L2**, which provides a 3N1S coordination sphere with a 12-membered ring, is the only one to fulfill all the required criteria.

L3 and **L4** are able to extract Cu^{II} and Cu^{I} from Aβ_{16} but produce higher amount of ROS than Cu–Aβ_{16} while **L5** can remove Cu^{I} from Aβ_{16} and slow down ROS production, but can get slowly oxidized with the Cu^{II} going back to Aβ_{16}.

Kinetic inertness of the Cu^{II}L2.

In addition to the ability to remove Cu from CuAβ_{16}, its ability to keep it (or not) in the biological medium is an important parameter to know. Here, we have shown that at pH 7.4, **L2** keeps Cu^{II} bound for several hours. In fact, the fate of the Cu^{II} once coordinated to **L2** is either further de-coordination to bind to another biomolecule or excretion from the brain as the complex, and this will mainly depend on the residence time of the metal ion inside the ligand. In contrast to what is required for ^{64}Cu ligands in PET imaging complexes, prevention of the transfer to other biomolecules is not an issue here. It has even been proposed as an interesting therapeutic strategy to transfer Cu from the extracellular space to the inside of cells in order to counterbalance the extracellular excess and intracellular deficiency proposed in AD.[58–61]

Further studies of such azamacrocycles could include enlarging the series with 14-, 15-, or 16-membered ring macrocycles, other donor atoms (O-containing macrocycles for instance), and the use of penta-coordinating N,S,O-containing macrocycles.[29,62] In addition, it is crucial to pay attention the interference of Zn^{II} in Cu removal from Aβ and redox silencing by **L*i***, as Zn^{II}, the other biometal ion present in millimolar quantity in the synaptic cleft, can impede Cu detoxification by chelators.[19,21,63] Such a study is currently in progress. Not only is the thermodynamic selectivity of Cu^{II} over Zn^{II} at play in this case (in contrast to previous reports[63–66]), but also kinetics. The results obtained, their interpretation and the mechanisms at play are very complex and will be reported in a forthcoming publication.

Experimental Section

All chemicals were purchased from Sigma-Aldrich, Fluorochem and TCI chemicals. Aβ_{40} (DAEFRHDSGYEVHHQKLVFFAEDVGSNKGAIIGLMVGGVV) and Aβ_{16} (DAEFRHDSGYEVHHQK) peptides were purchased from Genecust. **L1**–**L5** were synthesized by following the published protocol.[29,67] ^{65}Cu was obtained from a ^{65}Cu foil from Eurisotop. The no3pa ligand was purchased from EasyChelators.

Stock solutions: Stock solutions were prepared in Milli-Q water (resistivity: 18.2 MΩ.cm). HEPES buffer was prepared at an initial concentration of 500 mM, pH 7.4. $CuSO_4 \cdot 5H_2O$ was the source of Cu^{II}. A stock solution was prepared at 100 mM and titrated by UV-Vis spectroscopy. The concentration was determined at 800 nm with $\varepsilon_{800\,nm} = 12\ cm^{-1}\ M^{-1}$. A$\beta_{16}$ peptide and **L1**–**5** stock solutions of about 10 mM were prepared and titrated by UV-Vis spectroscopy. Aβ_{16} peptide concentration was determined using the Tyr chromophore with $\varepsilon_{276\,nm} = 1410\ cm^{-1}\ M^{-1}$ at acidic pH. The precise concentrations of **L1**–**5** were determined by Cu^{II} titration with a solution of $CuSO_4$ of known concentration using the d-d transition absorption of the complex to determine the equivalence point. **L5** was moderately soluble in water. **L5** was first dissolved in water; the supernatant was filtered and the soluble fraction was titrated. **L5** was soluble at about 5 mM. All stock solution were stored at 4 °C.

UV-visible spectrophotometry: UV-visible absorption spectra and ROS kinetic experiments were recorded on a Hewlett Packard Agilent 8453 or 8454 spectrophotometer at a controlled temperature of 25 °C in a 1 cm path length quartz cuvette, with 800 rpm

stirring. For competition absorption spectra, the samples were prepared in situ from stock solutions of **L1-5**, $A\beta_{16}$ and Cu^{II} diluted to 290, 290 and 240 μM respectively in 100 mM HEPES buffer, pH 7.4. The final volume in the cuvette was adjusted to 2 mL with Milli-Q water. For ROS kinetic experiments, samples were prepared in situ from stock solutions of **L1**–**5**, $A\beta_{16}$ and Cu^{II} at 1 mM diluted to 12 μM for **L1**–**5**, $A\beta_{16}$ and 10 μM for Cu^{II}, in 100 mM HEPES buffer, pH 7.4. Ascorbate was freshly prepared and diluted to 100 μM in the cuvette. The final volume in the cuvette was adjusted to 2 mL with Milli-Q water.

Electrochemical experiments: Electrochemical experiments were performed in an argon-flushed cell. A three-electrode setup was used, consisting of a glassy carbon (3 mm in diameter) disk as a working electrode, a platinum wire auxiliary electrode and a Saturated Calomel Electrode as reference electrode directly dipped into the solution. Cyclic voltammograms were recorded with an Autolab PGSTAT302N potentiostat piloted by EC-Lab software. The working electrode was carefully polished before each measurement on a red disk NAP with 1 μm AP–A suspension for at least 1 min (Struers). Additional support electrolyte was not added because of the high concentration of HEPES buffer in the solution. The scanning speed was 0.1 $V.s^{-1}$. The samples were prepared from stock solutions of **L1**–**5** and Cu^{II} diluted to the desired concentration.

Electron paramagnetic resonance: EPR spectra were recorded using an ELEXSYS Electron E500 Bruker spectrometer from 2600 to 3600 G, 0.5 mT amplitude modulation, approximately 9.5 GHz. The spectra were recorded using a microwave power of 5 mW and the experiments were carried out at 120 K using a liquid nitrogen cryostat.

For the competition experiments, in an Eppendorf tube, ^{65}Cu was first mixed with $A\beta_{16}$ (1.2 equiv.) in HEPES at pH 7.4. **L1**–**5** ligands were then added to the solution. The mixture was stirred for 10 min (unless stated otherwise in the figures' captions). Samples were frozen in a quartz tube after addition of 10% glycerol as a cryoprotectant and stored in liquid nitrogen until used.

XANES: Cu–K edge XANES spectra were recorded on the FAME beamline at the European Synchrotron Radiation Facility (ESRF, Grenoble, France) during an 15-shift session in Avril 2017 (experiment number A30-2 1125-CRG FAME-BM30B). The measurements were performed on mM solutions at low temperature (He-cryostat) in the fluorescence mode using a 30-element high-purity Ge detector (Canberra) in frozen liquid cells. The energy was calibrated with a Cu metallic foil spectra in transmission mode, with an energy set at 8979 eV corresponding to the maximum of the first derivative of the XANES transmission spectrum. For each sample, at least 3 XANES spectra were recorded and averaged. Samples for XANES measurements were prepared in the presence of 10% of glycerol as a cryoprotectant. A $Cu(SO_4)$ solution was used as source of Cu^{II} and the $CuA\beta_{16}$ complexes formed in situ were further reduced by dithionite 10 mM under an inert argon atmosphere, and in HEPES buffer 7.4 100 mM, according to previous reported methodology.[56,68] Possible drop of the pH due to dithionite addition was checked after the experiments and no acidic shift higher than +0.2 pH unit was measured.

Note that in our study, we have focused on Cu^{I} complexes for two main reasons: i) For d^{10} ion, X-ray absorption spectroscopy is a leading if not the sole investigation method in contrast to Cu^{II} and ii) for Cu^{II} species, photo-reduction is a main issue to deal with,[69] that we were not able to solve during the beamtime allocated.

ROS measurement: The decrease of the ascorbate UV absorption band at $\lambda_{max}=265$ nm ($\varepsilon=14\ 500\ M^{-1}.cm^{-1}$), corrected at 800 nm, was plotted against time. The samples were prepared in situ from stock solutions at 1 mM diluted to 12 μM for ***Li*** and $A\beta_{16}$ and to 10 μM for Cu^{II}, in 100 mM HEPES buffer, pH 7.4. The final volume in the cuvette was adjusted to 2 mL with Milli-Q water.

The ROS experiments were performed following three different procedures: starting from Cu^{II}, starting from Cu^{I} and starting from a mixture of Cu^{I} and Cu^{II}. For the first experiment, ***Li*** was added to a Cu^{II} or $Cu^{II}+A\beta_{16}$ mixture under aerobic conditions and then ascorbate was introduced in the cuvette. For the second one, ***Li*** was injected with Hamilton syringe to Cu^{I} or $Cu^{I}+A\beta_{16}$ in a sealed cuvette under anaerobic conditions. Then the cuvette was open to air and air was bubbled in the cuvette to ease the fast solubilization of dioxygen. The Cu^{I} was generated by the in-situ reduction of Cu^{II} with ascorbate. All the solution were previously degassed with argon 15 min before being introduced in the sealed UV-vis cuvette under argon. For Figure S14, instead of bubbling air in the cuvette, 500 μL of HEPES buffer (100 mM, pH 7.4) saturated with O_2 were added in the cuvette. For the last one (mixture of Cu^{I} and Cu^{II}), ascorbate was introduced first into the cuvette under aerobic conditions, then either Cu^{II} or $Cu^{II}+A\beta_{16}$ was added. When the concentration of ascorbate was reaching about 1.2, ***Li*** was added.

N.B. The level of O_2 was probed by using a Clark electrode, during the Cu(Aβ)-induced ascorbate consumption to ensure that no bias occurs during the UV-Vis experiments of ascorbate consumption. The level of O_2 starts at 0.25 ± 0.01 mM and decreases by less than 15% along the same kinetics than ascorbate consumption, and increases back to the initial level once the ascorbate has been fully consumed (Figure S18 and related comments in the Supporting Information). This indicates that the level of O_2 is not limiting for the whole reaction at play.

Acknowledgements

C.H., C.E., K.P.M. and E.A.B. thank the ERC aLzINK-Contract no. 638712 for financial support. C.E. thanks ANR project Copperation for financial support. The Ecole normale supérieure PSL is acknowledged for M.D.'s PhD grant. C.H. and E.A.B. warmly acknowledge the human support of FAME beamline at ESRF (project A30-2 1125-CRG FAME-BM30B) and collaborators who helped in recording the data (A. Conte Daban, Dr. F. Collin, Dr. S. Sayen, and Prof. Guillon). Dr. P. Dorlet is warmly acknowledged for providing simulations of the Cu^{II}***Li*** EPR spectra. Francois Gu is acknowledged for the preliminary experiments he performed. K.P.M dedicates this work to Hangi Celestin Malikidogo.

Conflict of Interest

There are no conflicts to declare

Data Availability Statement

The data that support the findings of this study are available from the corresponding author upon reasonable request.

Keywords: Alzheimer's disease · copper · EPR · macrocycles · oxidative stress

[1] Alzheimer's Association, *Alzheimer's Dementia* **2017**, *13*, 325–373.
[2] N. N. Nalivaeva, A. J. Turner, *Br. J. Pharmacol.* **2019**, *176*, 3447–3463.
[3] J. Hardy, G. Higgins, *Science* **1992**, *256*, 184–185.
[4] J. Hardy, D. J. Selkoe, *Science* **2002**, *297*, 353–356.
[5] C. Hureau, *Coord. Chem. Rev.* **2012**, *256*, 2164–2174.
[6] E. Atrián-Blasco, P. Gonzalez, A. Santoro, B. Alies, P. Faller, C. Hureau, *Coord. Chem. Rev.* **2018**, *371*, 38–55.
[7] M. A. Lovell, J. D. Robertson, W. J. Teesdale, J. L. Campbell, W. R. Markesbery, *J. Neurol. Sci.* **1998**, *158*, 47–52.
[8] L. M. Miller, Q. Wang, T. P. Telivala, R. J. Smith, A. Lanzirotti, J. Miklossy, *J. Struct. Biol.* **2006**, *155*, 30–37.
[9] J. Dong, C. S. Atwood, V. E. Anderson, S. L. Siedlak, M. A. Smith, G. Perry, P. R. Carey, *Biochemistry* **2003**, *42*, 2768–2773.
[10] J. Everett, F. Lermyte, J. Brooks, V. Tjendana-Tjhin, G. Plascencia-Villa, I. Hands-Portman, J. M. Donnelly, K. Billimoria, G. Perry, X. Zhu, P. J. Sadler, P. B. O'Connor, J. F. Collingwood, N. D. Telling, *Sci. Adv.* **2021**, *7*, eabf6707.
[11] M. P. Cuajungco, L. E. Goldstein, A. Nunomura, M. A. Smith, J. T. Lim, C. S. Atwood, X. Huang, Y. W. Farrag, G. Perry, A. I. Bush, *J. Biol. Chem.* **2000**, *275*, 19439–19442.
[12] A. C. Leskovjan, A. Lanzirotti, L. M. Miller, *NeuroImage* **2009**, *47*, 1215–1220.
[13] C. Cheignon, M. Tomas, D. Bonnefont-Rousselot, P. Faller, C. Hureau, F. Collin, *Redox Biol.* **2018**, *14*, 450–464.
[14] C. Hureau in *Encyclopedia of Inorganic and Bioinorganic Chemistry* (Ed.: R. A. Scott), John Wiley & sons, Inc, **2019**, 1–14.
[15] B. Alies, E. Renaglia, M. Rózga, W. Bal, P. Faller, C. Hureau, *Anal. Chem.* **2013**, *85*, 1501–1508.
[16] A. Conte-Daban, V. Borghesani, S. Sayen, E. Guillon, Y. Journaux, G. Gontard, L. Lisnard, C. Hureau, *Anal. Chem.* **2017**, *89*, 2155–2162.
[17] C. Cheignon, M. Jones, E. Atrián-Blasco, I. Kieffer, P. Faller, F. Collin, C. Hureau, *Chem. Sci.* **2017**, *8*, 5107–5118.
[18] E. Atrián-Blasco, M. del Barrio, P. Faller, C. Hureau, *Anal. Chem.* **2018**, *90*, 5909–5915.
[19] C. Esmieu, D. Guettas, A. Conte-Daban, L. Sabater, P. Faller, C. Hureau, *Inorg. Chem.* **2019**, *58*, 13509–13527.
[20] M. G. Savelieff, G. Nam, J. Kang, H. J. Lee, M. Lee, M. H. Lim, *Chem. Rev.* **2019**, *119*, 1221–1322.
[21] Y. Liu, M. Nguyen, A. Robert, B. Meunier, *Acc. Chem. Res.* **2019**, *52*, 2026–2035.
[22] A. Conte-Daban, M. Beyler, R. Tripier, C. Hureau, *Chem. Eur. J.* **2018**, *24*, 8447–8452.
[23] R. E. Mewis, S. J. Archibald, *Coord. Chem. Rev.* **2010**, *254*, 1686–1712.
[24] J. Wang, K. Wang, Z. Zhu, Y. He, C. Zhang, Z. Guo, X. Wang, *RSC Adv.* **2019**, *9*, 14126–14131.
[25] T. Chen, X. Wang, Y. He, C. Zhang, Z. Wu, K. Liao, J. Wang, Z. Guo, *Inorg. Chem.* **2009**, *48*, 5801–5809.
[26] Y. Yang, T. Chen, S. Zhu, X. Gu, X. Jia, Y. Lu, L. Zhu, *Integr. Biol.* **2015**, *7*, 655–662.
[27] M. M. Bernardo, M. J. Heeg, R. R. Schroeder, L. A. Ochrymowycz, D. B. Rorabacher, *Inorg. Chem.* **1992**, *31*, 191–198.
[28] D. B. Rorabacher, *Chem. Rev.* **2004**, *104*, 651–698.
[29] J. Hormann, C. Perera, N. Deibel, D. Lentz, B. Sarkar, N. Kulak, *Dalton Trans.* **2013**, *42*, 4357–4360.
[30] J. V. Dagdigian, V. McKee, C. A. Reed, *Inorg. Chem.* **1982**, *21*, 1332–1342.
[31] K. P. Balakrishnan, T. A. Kaden, L. Siegfried, A. D. Zuberbühler, *Helv. Chim. Acta* **1984**, *67*, 1060–1069.
[32] T. L. Walker, S. Mula, W. Malasi, J. T. Engle, C. J. Ziegler, A. van der Est, J. Modarelli, M. J. Taschner, *Dalton Trans.* **2015**, *44*, 20200–20206.
[33] J.-X. Guo, S.-Y. Wu, Y.-J. Luo, Y.-M. Fan, Q.-S. Zhu, *Comput. Theor. Chem.* **2020**, *1189*, 112952.
[34] J. Peisach, W. E. Blumberg, *Arch. Biochem. Biophys.* **1974**, *165*, 691–708.
[35] S. T. Marcus, P. V. Bernhardt, L. Grøndahl, L. R. Gahan, *Polyhedron* **1999**, *18*, 3451–3460.
[36] S. K. Hoffmann, J. Goslar, S. Lijewski, A. Zalewska, *J. Magn. Reson.* **2013**, *236*, 7–14.
[37] U. Sakaguchi, A. W. Addison, *J. Am. Chem. Soc.* **1977**, *99*, 5189–5190.
[38] D. Poger, C. Fillaux, R. Miras, S. Crouzy, P. Delangle, E. Mintz, C. Den Auwer, M. Ferrand, *J. Biol. Inorg. Chem.* **2008**, *13*, 1239–1248.
[39] K. Fujisawa, S. Imai, S. Suzuki, Y. Moro-oka, Y. Miyashita, Y. Yamada, K.-i. Okamoto, *J. Inorg. Biochem.* **2000**, *82*, 229–238.
[40] K. Chen, S. Yuldasheva, J. E. Penner-Hahn, T. V. O'Halloran, *J. Am. Chem. Soc.* **2003**, *125*, 12088–12089.
[41] R. A. Pufahl, C. P. Singer, K. L. Peariso, S. J. Lin, P. J. Schmidt, C. J. Fahrni, V. C. Culotta, J. E. Penner-Hahn, T. V. O'Halloran, *Science* **1997**, *278*, 853–856.
[42] D. Coucouvanis, C. N. Murphy, S. K. Kanodia, *Inorg. Chem.* **1980**, *19*, 2993–2998.
[43] F. Yu, J. E. Penner-Hahn, V. L. Pecoraro, *J. Am. Chem. Soc.* **2013**, *135*, 18096–18107.
[44] L. S. Kau, D. J. Spira-Solomon, J. E. Penner-Hahn, K. O. Hodgson, E. I. Solomon, *J. Am. Chem. Soc.* **1987**, *109*, 6433–6442.
[45] G. A. Stergioudis, S. C. Kokkou, P. J. Rentzeperis, P. Karagiannidis, *Acta Crystallogr. Sect. C* **1987**, *43*, 1685–1688.
[46] L. M. P. Lima, D. Esteban-Gómez, R. Delgado, C. Platas-Iglesias, R. Tripier, *Inorg. Chem.* **2012**, *51*, 6916–6927.
[47] K. S. Woodin, K. J. Heroux, C. A. Boswell, E. H. Wong, G. R. Weisman, W. Niu, S. A. Tomellini, C. J. Anderson, L. N. Zakharov, A. L. Rheingold, *Eur. J. Inorg. Chem.* **2005**, *2005*, 4829–4833.
[48] L. Siegfried, T. A. Kaden, *Helv. Chim. Acta* **1984**, *67*, 29–38.
[49] H. Kozlowski, M. Luczkowski, M. Remelli, D. Valensin, *Coord. Chem. Rev.* **2012**, *256*, 2129–2141.
[50] A. Conte-Daban, A. Day, P. Faller, C. Hureau, *Dalton Trans.* **2016**, *45*, 15671–15678.
[51] R. De Ricco, D. Valensin, S. Dell'Acqua, L. Casella, C. Hureau, P. Faller, *ChemBioChem* **2015**, *16*, 2319–2328.
[52] S. Chassaing, F. Collin, P. Dorlet, J. Gout, C. Hureau, P. Faller, *Curr. Top. Med. Chem.* **2012**, *12*, 2573–2595.
[53] C. Esmieu, R. Balderrama-Martínez-Sotomayor, A. Conte-Daban, O. Iranzo, C. Hureau, *Inorg. Chem.* **2021**, *60*, 1248–1256.
[54] V. Borghesani, B. Alies, C. Hureau, *Eur. J. Inorg. Chem.* **2018**, *2018*, 7–15.
[55] B. Alies, I. Sasaki, O. Proux, S. Sayen, E. Guillon, P. Faller, *C. Hureau, Chem. Commun.* **2013**, *49*, 1214–1216.
[56] E. Atrián-Blasco, E. Cerrada, A. Conte-Daban, D. Testemale, P. Faller, M. Laguna, C. Hureau, *Metallomics* **2015**, *7*, 1229–1232.
[57] E. A. Ambundo, M.-V. Deydier, A. J. Grall, N. Aguera-Vega, L. T. Dressel, T. H. Cooper, M. J. Heeg, L. A. Ochrymowycz, D. B. Rorabacher, *Inorg. Chem.* **1999**, *38*, 4233–4242.
[58] M. Okafor, P. Gonzalez, P. Ronot, I. El Masoudi, A. Boos, S. Ory, S. Chasserot-Golaz, S. Gasman, L. Raibaut, C. Hureau, N. Vitale, P. Faller, *Chem. Sci.* **2022**, *13*, 11829–11840.
[59] P. S. Donnelly, A. Caragounis, T. Du, K. M. Laughton, I. Volitakis, R. A. Cherny, R. A. Sharples, A. F. Hill, Q.-X. Li, C. L. Masters, K. J. Barnham, A. R. White, *J. Biol. Chem.* **2008**, *283*, 4568–4577.
[60] P. J. Crouch, L. W. Hung, P. A. Adlard, M. Cortes, V. Lal, G. Filiz, K. A. Perez, M. Nurjono, A. Caragounis, T. Du, K. Laughton, I. Volitakis, A. I. Bush, Q.-X. Li, C. L. Masters, R. Cappai, R. A. Cherny, P. S. Donnelly, A. R. White, K. J. Barnham, *Proc. Natl. Acad. Sci. USA* **2009**, *106*, 381–386.
[61] P. J. Crouch, M. S. Savva, L. W. Hung, P. S. Donnelly, A. I. Mot, S. J. Parker, M. A. Greenough, I. Volitakis, P. A. Adlard, R. A. Cherny, C. L. Masters, A. I. Bush, K. J. Barnham, A. R. White, *J. Neurochem.* **2011**, *119*, 220–230.
[62] J. Hormann, M. van der Meer, B. Sarkar, N. Kulak, *Eur. J. Inorg. Chem.* **2015**, *2015*, 4722–4730.
[63] E. Atrián-Blasco, A. Conte-Daban, C. Hureau, *Dalton Trans.* **2017**, *46*, 12750–12759.
[64] A. E. Behar, L. Sabater, M. Baskin, C. Hureau, G. Maayan, *Angew. Chem. Int. Ed.* **2021**, *60*, 24588–24597; *Angew. Chem.* **2021**, *133*, 24793–24802.
[65] E. Atrián-Blasco, E. Cerrada, P. Faller, M. Laguna, C. Hureau, *Metallomics* **2019**, *11*, 1154–1161.
[66] W. Zhang, Y. Liu, C. Hureau, A. Robert, B. Meunier, *Chem. Eur. J.* **2018**, *24*, 7825–7829.
[67] A. H. Alberts, J.-M. Lehn, D. Parker, *J. Chem. Soc. Dalton Trans.* **1985**, 2311–2317.
[68] C. Hureau, V. Balland, Y. Coppel, P. L. Solari, E. Fonda, P. Faller, *J. Biol. Inorg. Chem.* **2009**, *14*, 995–1000.
[69] F. Stellato, R. Chiaraluce, V. Consalvi, E. De Santis, G. La Penna, O. Proux, G. Rossi, S. Morante, *Metallomics* **2019**, *11*, 1401–1410.

Manuscript received: November 24, 2022
Accepted manuscript online: January 6, 2023
Version of record online: January 26, 2023